Spring 3-24-2023

Purification and Kinetic Characterization of Mutant R111V Human Cytosolic Malate Dehydrogenase

Jackson DeMartino
Providence College

Purification and kinetic characterization of mutant R111V human cytosolic malate dehydrogenase

Received for publication May 13th, 2022

Jackson DeMartino, Tyler Stack, and Kathleen Cornely

From the Department of Chemistry and Biochemistry, Providence College, Providence, RI 02918

Metabolic profiling for a variety of cancerous cells indicate significant increases in the levels of glucose consumption. To support uncontrolled cell division, cancer cells also present an uncoupling of glycolysis from the citric acid cycle to promote glucose carbons to the synthesis of biomass, therefore, requiring a constant supply of NAD^+. Recent studies indicate that cancer cells exhibit upregulated cytosolic malate dehydrogenase (MDH1) activity, which catalyzes the conversion of oxaloacetate to malate with the oxidation of NADH, generating NAD^+. Given its increased activity, MDH1 may serve as a valuable target for treating cancer. Here we report the effects on enzyme catalytic efficiency and specificity induced by the point-substitution, R111V, within the flexible loop of MDH1-isoform-3, constructed by site-directed mutagenesis. The mutant protein was purified by Ni-NTA chromatography and analyzed by modified Michaelis-Menten kinetics to determine changes in kinetic constants with natural substrate, OAA, and non-preferred substrate, phenylpyruvate. We found that this mutation does not significantly change enzyme specificity or catalytic efficiency for phenylpyruvate, as shown in k_{cat} values of 1050 ± 50 and 1.1 ± 0.1 × 10^3 $M^{-1}s^{-1}$ for mutant and wild type enzyme, respectively. However, we report changes in k_{sp} for preferred substrate, OAA, with values of 1.2 ± 0.1 × 10^7 and 5.9 ± 0.1 × 10^7 $M^{-1}s^{-1}$ for mutant and wild type enzymes, respectively. In addition, we report a Hill coefficient (n = 2) for wild type enzyme with OAA that suggests cooperativity between subunits of MDH1, which challenges preceding classification of the enzyme as non-cooperative.

The alarming increase in cancer diagnoses observed this past decade has prompted the need for novel therapeutics that selectively target cancer cells in an efficient manner to decrease their proliferative rates. Previous studies indicate that cancer cells show increased rates of glucose consumption to support uncontrolled cell proliferation. This requires cancer cells to uncouple glycolysis from the citric acid cycle for glucose carbons to be diverted to the production of biomass, including that of DNA, RNA, fatty acids, and proteins necessary for cell growth and division. This metabolic pattern has been titled the Warbug Effect, referring to the increased levels of glucose uptake and anaerobic fermentation observed in cancer cells (1).

It follows that for glycolysis to be at the heightened rates exhibited by cancer cells, there must be sufficient supplies of NAD^+. In the past, the primary method of NAD^+ regeneration in cancer cells was thought to be via lactic acid fermentation. However, because of the diversion of glucose carbons to pathways for biomass synthesis, less available pyruvate for lactate dehydrogenase (LDH) suggests that the enzyme must not be the sole player in NAD^+ regeneration.

Research has suggested that both LDH and cytosolic malate dehydrogenase (MDH1), the enzyme responsible for operating the malate-aspartate shuttle for the transport of NADH to the mitochondria, work to increase supplies of NAD^+ (2). In fact, studies have indicated that both LDH and MDH1 have significantly greater levels of activity in cancerous tissue compared to healthy, while greater MDH1 expression has been correlated with poor prognosis in patients suffering from both non-small cell carcinoma and breast cancer (3,4). Importantly, these studies demonstrate that in patients presenting non-small cell carcinoma, MDH1 activity is comparably as high as mitochondrial MDH (MDH2), however only higher levels of MDH1 is correlated with poor prognosis. This may suggest that MDH1 is a more valuable therapeutic target than the mitochondrial MDH2. Therefore, it is of great interest to further understand how changes in MDH1 structure and function can contribute to the progression of cancers like non-small cell carcinoma.

Here we present the purification and enzymatic analysis of mutant R111V MDH1, isoform 3 (MDH1-3) (EC 1.1.1.37) enzyme including its specificity and catalytic efficiency upon preferred and non-preferred substrates, OAA and phenylpyruvate, respectively. Prior to enzyme characterization, it was hypothesized that the R111V mutation within the flexible loop (which controls substrate discrimination) may decrease enzyme specificity to allow for catalysis upon the larger substrate, phenylpyruvate, by introduction of the smaller, hydrophobic residue, valine. However, we report that the

R111V mutation does lower enzyme specificity and efficiency for substrate OAA compared to wild type MDH1, as shown by lower k_{sp} values. Additionally, we show that the mutation produces no significant change in the substrate specificity for phenylpyruvate, however, both wild type and mutant protein present enzymatic activity for the non-preferred substrate. This study provides compelling evidence that the R111V mutation introduces changes to the kinetic behavior of MDH1, which further reiterates the importance of mutagenic studies in gaining a deeper understanding of the enzyme's role in metabolic changes observed in cancerous states.

Results

Multiple sequence alignment of MDH1-3 isoform

In order to select an interesting mutation for this study, a multiple sequence alignment with the cytosolic MDH1-3 isoform (UniProt ID: P40925-3) was first performed against several variants from a diverse set of genera (5). This allowed for identification of multiple highly conserved and immutable residues, shown in Table 1, that are crucial to enzymatic function.

The mutation of choice was limited to the flexible loop region, and a keen focus was diverted to residues involved in catalysis and substrate binding. PyMOL modeling of the MDH1-3 isoform revealed Arg 111 to be a viable candidate for mutation (Fig. 1*A*) (6). The R111 residue neighbors R110, which is involved in OAA binding. It was decided that mutation of R111 to valine may change the enzymatic properties of the wild type MDH1-3 isoform, possibly inducing an increased efficiency to catalyze reaction with pyruvate, an important consideration for increased anaerobic fermentation in cancer cells (Fig. 1*B*).

Using Alpha Fold predicted mutant MDH1-3 structure for simulated docking of pyruvate with Swiss Dock

In order to visualize the chosen mutation, mutant R111V MDH1-3 was folded using Alpha Fold (7). With the resulting protein structure, the appropriate coordinates within the active site were determined to accommodate substrate phenylpyruvate docking via PyMOL modeling (Fig 2*A*). The PDB file was then processed through Swiss Dock with these constraints to simulate phenylpyruvate binding to mutant R111V MDH1-3 active site (8).

The clusters that reasonably depicted phenylpyruvate docking in respect to the active site were chosen based on proximity and orientation to the active site modeled with Chimera (Fig. 2*B*) (9). Free energy changes, ΔG, associated with substrate binding were averaged for each cluster. The R111V MDH1-3 mutant showed an average ΔG for phenylpyruvate docking of -6.3 ± 0.3 kJ/mol, with a minimum ΔG of -7.2 kJ/mol. This value was not dramatically different from average ΔG values associated with phenylpyruvate and oxaloacetate docking for WT MDH1-3 when subject to the same process through Alpha Fold and docking by Swiss Dock. In fact, wild type MDH1-3 presented an average ΔG of -6.6 and -6.4 kJ/mol when analyzed by oxaloacetate and phenylpyruvate docking, respectively.

Table 1

Highly conserved residues across MDH1-3 variants

Residue	Residue number in P49025-3
G	29
G	32
G	70
R	110
G	113
M	114
R	116
N	123
N	149
P	150
L	176
D	177
R	180
G	203
G	249
S	260
P	207

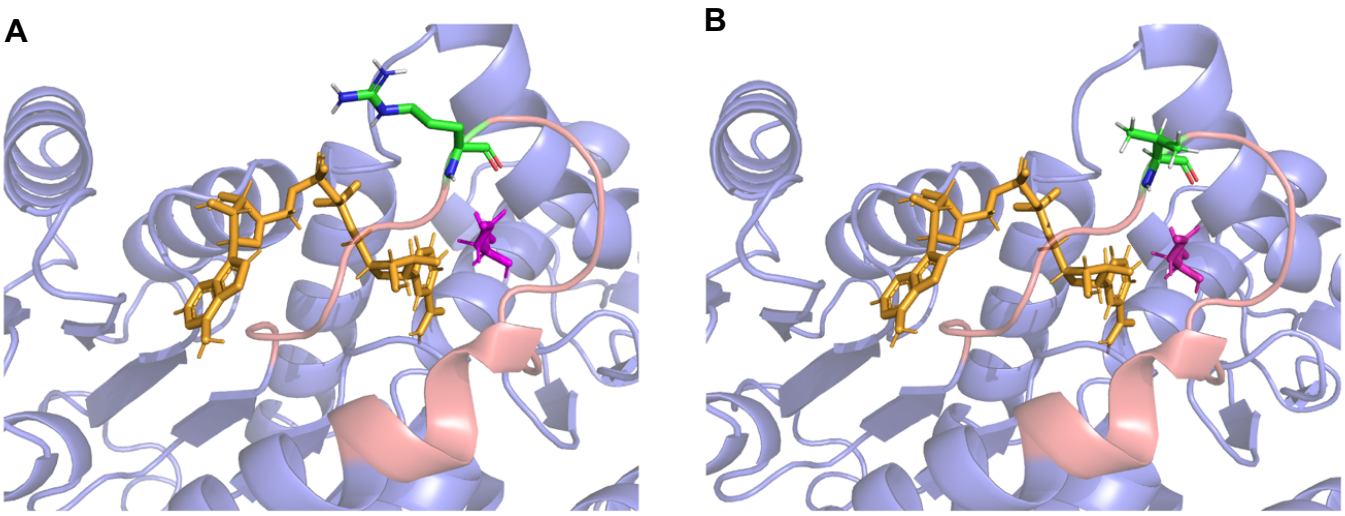

Figure 1. Visual molecular modeling of MDH1-3 active site for both wild type and R111V mutant. *A,* wild type MDH1-3 active site showing substrate malate (magenta), substrate NAD^+ (gold), and residue R111 (in stick form, colored by element according to IUPAC standards) in respect to active flexible loop (highlighted in red). *B,* mutant R111V in same color scheme with V111 residue shown in stick form, colored by element. Both models were generated with PyMOL.

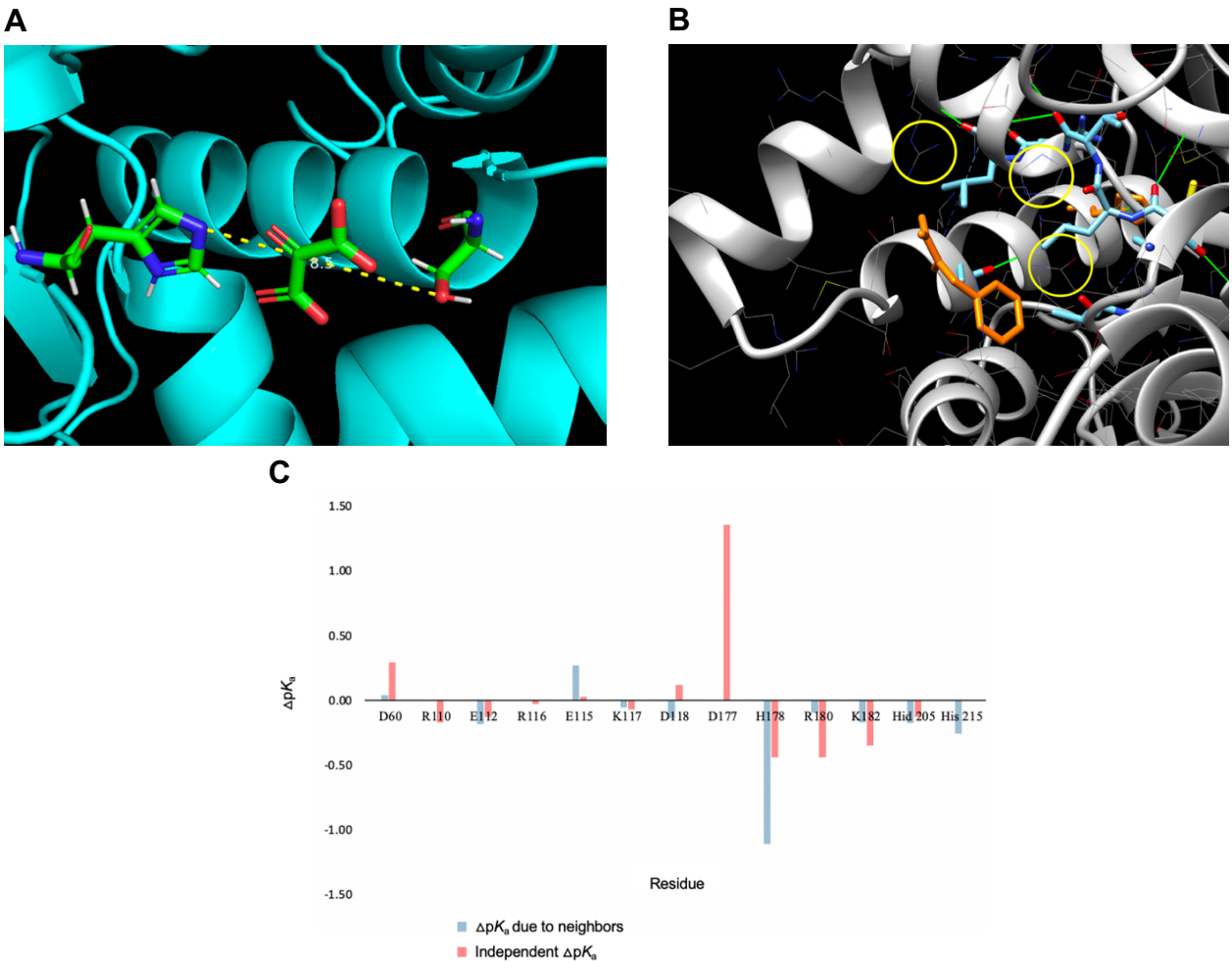

Figure 2. Molecular and computational analysis of mutant R111V MDH1-3. *A*, center of active site between flanking residues H205 and S259 modeled in PyMOL. *B*, docking of non-preferred substrate phenylpyruvate (gold) in proximity to catalytic residues H205, N149, and R180 (circled), in a favorable orientation as computed by Swiss Dock and modeled on Chimera. *C*, ΔpK_a values for important titratable residues between mutant R111V MDH1-3 and wild type enzyme (wild type – mutant), considering the effects of neighboring residues (blue) and independent changes (red) as calculated by H++.

Determining pK_a values for titratable residues in mutant MDH1-3 using H++

In order to determine changes in the acidic environments for residues involved in catalysis and ligand binding induced by the R111V mutation, the predicted mutant structure was processed by H++ (10). The program provided pK_a values of all titratable residues, both independent pK_a values and those induced by neighboring residues. Keen attention was directed to residues in close proximity to the R111V mutation and those involved in catalysis and substrate binding. The pK_a data for was translated into ΔpK_a values between wild type and mutant R111V MDH1-3 (Table 2) and the data displayed in Figure 2*C* visually displays the overall changes. Importantly, previously identified catalytic residues, D177, H205, R110, and D60 present significant changes in their pK_a values, both independently and collectively.

Nanodrop™ analysis of wild type pET28a DNA

Following plasmid miniprep of WT MDH1-3 pET28a, the concentration of collected plasmid DNA was analyzed via Nanodrop™ spectrophotometry. The eluted DNA presented a concentration of 908.9 ng/µL with 260/230 and 260/280 ratios of 2.58 and 2.24, respectively (Fig. 3). According to the manufacturer's guidelines, both ratios were outside of the acceptable ranges (260/280 at 1.8 and 260/230 between 2.0-2.2). Therefore, the recorded ratios are higher than acceptable (Thermo Fisher Scientific 1009 Technical Bulletin). A possible rationale for the high 260/280 is the content of specific nitrogenous bases with higher absorbances at 260 nm. This ratio is a weighted average of the nitrogenous bases present, with adenine and uracil having the largest absorbances (4.50 and 4.0, respectively). Therefore, the plasmid DNA sample may have a high adenine content, accounting for the high 260/280 ratio.

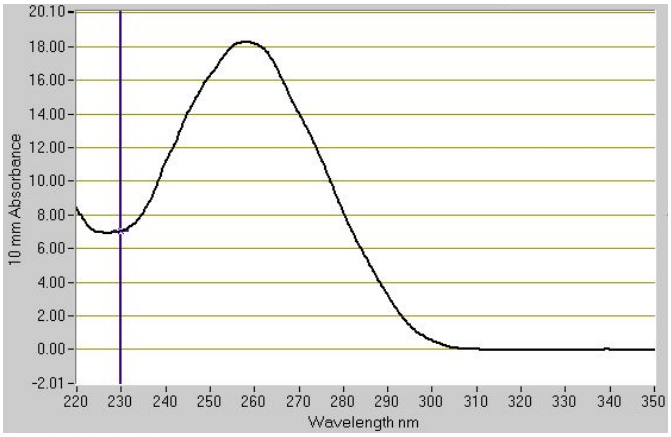

Figure 3. Spectrophotometry of WT plasmid DNA solution by NanoDrop™. The absorbance curve of the WT MDH1-3 pET28a plasmid DNA solution showed a maximum absorbance at 260 nm. The curve resembles that of a pure nucleic acid sample, with a trough at 230 nm.

Table 2

ΔpK_a values of selected, titratable residues of wild type and mutant R111V MDH1-3.

Residue	ΔpK_a (neighbors)	ΔpK_a (independent)
D60[a]	0.04	0.29
R110[c]	0.0	-0.17
E112[b]	-0.018	-0.13
E115[b]	0.27	-0.026
R116[c]	0.00	0.029
K117[b]	-0.055	-0.067
D118[b]	-0.13	0.12
D177[a]	0.0	1.3
H178[a]	-1.1	-0.43
R180[a]	-0.096	-0.44
K182[a]	-0.17	-0.34
Hid 205[a]	-0.17	-0.12
His 215[c]	-0.26	0.00

[a] Catalytically active residues
[b] Residues in proximity to mutation
[c] Residues involved in ligand binding

Restriction digest of wild type MDH1-3 plasmid DNA

Verification of collected wild type MDH1-3 pET28a plasmid DNA was completed via double restriction digest with BglI and NcoI restriction enzymes (New England Biolabs). Comparing the resulting gel electrophoresis of digested and non-digested plasmid to the virtual digest extrapolated from Benchling confirmed that the purification of wild type plasmid was successful (Fig. 4).

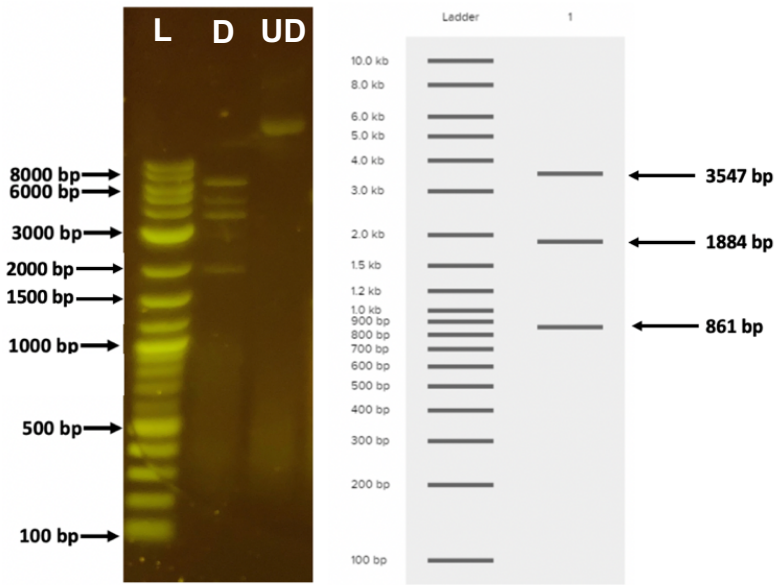

Figure 4. Restriction digest of wild type plasmid. Electrophoresis results from running the digested and undigested reactions (left) are shown in respect to the virtual digest (right). The lanes exhibited contain 1 kb ladder (L), digested reaction (D), and undigested reaction (UD).

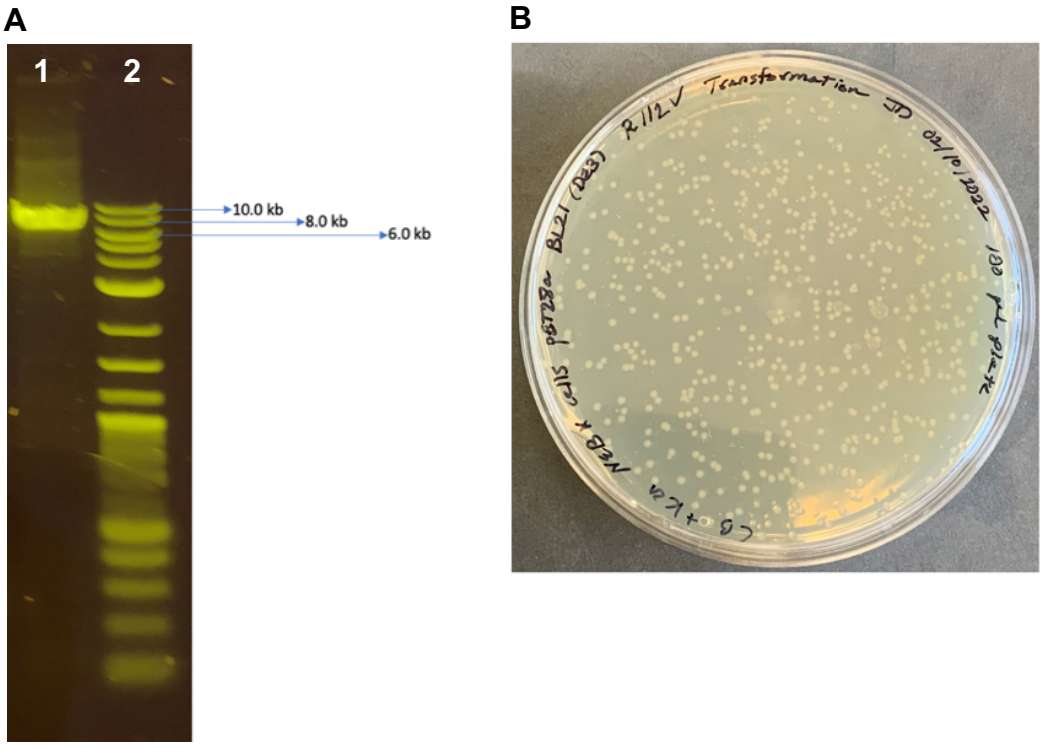

Figure 5. Site-directed mutagenesis of wild type pET28a MDH1-3 and transformation of competent cells. *A,* resulting electrophoresis of the site directed mutagenesis reaction with wild type MDH1-3 pET28a plasmid (labeled as lane 1). Reaction is compared to 1 kb plus ladder (lane 2), with reference bands marked. *B*, sufficient growth of transformants seen for 100 µL of undiluted transformation plated.

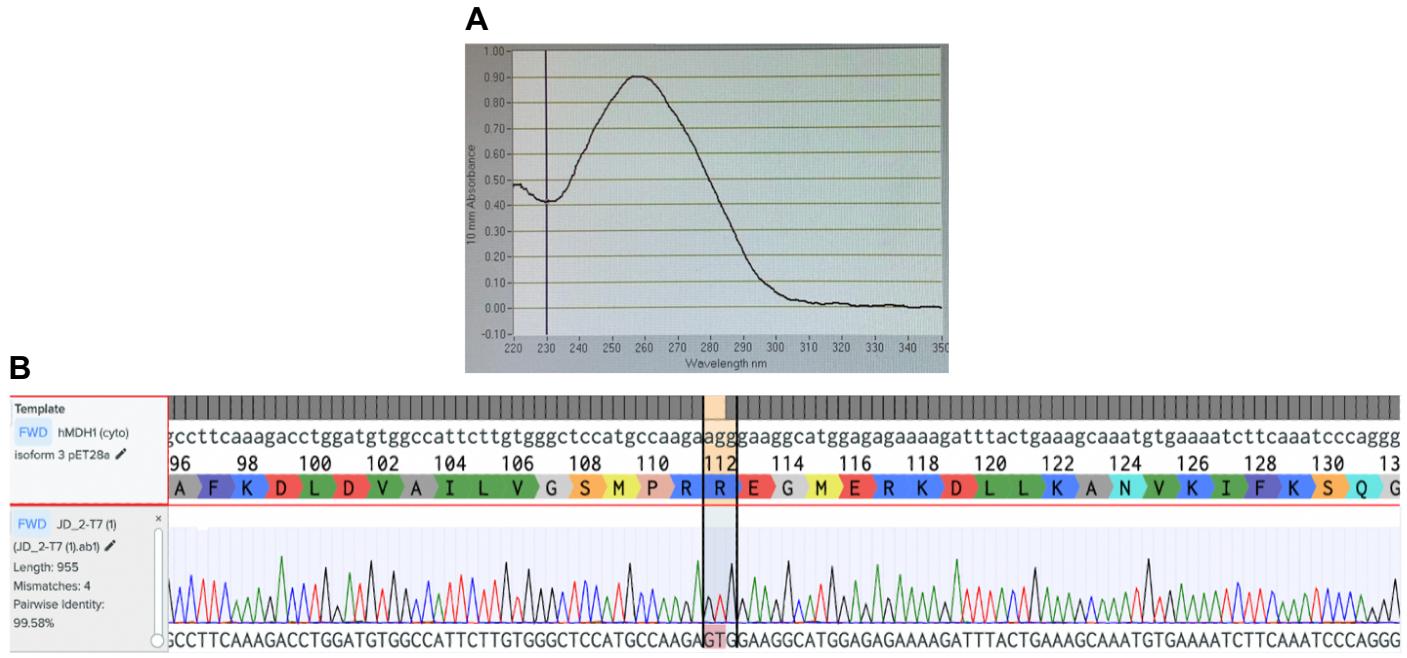

Figure 6. Sanger sequencing of collected mutant R111V pET28a MDH1-3 plasmid DNA. *A,* NanoDrop™ analysis of mutant R111V pET28a plasmid DNA collected via plasmid miniprep. *B*, alignment of template, WT pET28a MDH1-3 plasmid DNA (top) and mutant R112V mutant plasmid DNA (bottom). Bracketed is the R112 residue (corresponding to R111 in MDH1-3 sequence) with GT nucleotide substitutions highlighted in red.

The virtual digest predicted bands of length 1884 (with BglI), 861, and 3547 (with NcoI). As shown in Figure 4, bands are present at the approximate 4000 bp mark (corresponding to 3547 fragment) and 2000 bp (1884 bp fragment) in the lane with the digest mixture present. Faintly, a band is present between 900 and 800 bp (corresponding to the 861 bp fragment). There are additional bands present at approximately 6000 bp and 5000 bp which likely reflect partially digested plasmid. In the lane with the uncut reaction, there is a band outside of the ladder range, which may suggest that the intact plasmid did not travel to its respective position of 6292 bp.

Site directed mutagenesis using mutagenic primers

In order to insert the chosen mutation, R111V, into the pET28a MDH1-3 plasmid, a site directed mutagenesis procedure with exponential amplification via PCR was carried out using primers designed by New England Biolabs. The PCR product showed an appropriate length compared to the WT pET28a MDH1-3 plasmid of 6292 bp when analyzed by gel electrophoresis (Fig. 5*A*). While this does not confirm that the mutagenesis was successful, it does suggest that PCR amplified the product from the mutagenesis reaction mixture as shown by the band thickness.

Kinase, ligase, and DpnI treatment and transformation with mutant pET28a MDH1-3 plasmid

In order to return the PCR product to circular form and isolate it from non-mutated template DNA prior to transformation, a KLD treatment was performed. The circularized mutant plasmid DNA was then used to transform NEB 5-α competent cells. Sufficient growth, even approaching overgrowth of transformants was seen after overnight incubation of the transformation mix (Fig. 5*B*). Growth of transformants suggests that the KLD and transformation procedures were successful, given that the colonies present must express the kanamycin resistance gene to grow on the agar media.

Plasmid-miniprep of mutant pET28a MDH1-3 plasmid

Purification of the mutant R111V pET28a MDH1-3 plasmid by miniprep proved to be successful via NanoDrop™ spectrophotometry. The resulting absorption curve indicates that the DNA collected from

the performed miniprep is of acceptable quality, with the spectra (Fig. 6*A*) exhibiting acceptable 260/230 and 260/280 ratios of 2.17 and 1.85, respectively. The curve also shows an expected peak at 260 nm and a trough at 230 nm, indicating successful purification of a nucleic acid sample.

GeneWiz Sequencing of collected mutant pET28a MDH1-3 plasmid DNA

Mutant R111V pET28a MDH1-3 plasmid DNA was sequenced by GeneWiz in order to verify that the plasmid DNA collected was mutated with the correct substitutions and possessed an intact plasmid. The collected sample of mutant plasmid DNA exhibited the GT nucleotide mutations at the 5405 and 5406 base locations within the plasmid sequence (Fig. 6*B*). In addition, the sequence presents sufficient quality indicated by the high pairwise identity of 99.58% and a low mismatch count of 4 as calculated by Benchling.

Transformation of competent XJb (DE3) cells with mutant pET28a MDH1 plasmid DNA

Competent XJb (DE3) cells were transformed with mutant R111V pET28a plasmid DNA to prepare for the overexpression process. Transformation of competent cells proved successful with sufficient transformant growth seen after overnight incubation, exhibiting a transformation efficiency of 4.6×10^3 colonies/µg plasmid DNA (Fig. 7).

Cultures made from these transformants were subject to an IPTG overexpression procedure to induce expression of the mutant R111V MDH1-3 protein for eventual purification. The harvested cells were lysed in preparation for Ni-NTA chromatographic purification.

Mutant MDH1-3 protein purification by Ni-NTA chromatography

In order to verify that the Ni-NTA chromatography successfully washed unwanted protein, the absorbances of each eluent were measured at 280 nm (Table 3). As apparent from the decreasing trend of absorbances at each wash step and the high absorbance upon protein elution, it can be suggested that the chromatography was successful in purifying the target R111V MDH1-3 mutant protein, pending confirmation by SDS-PAGE.

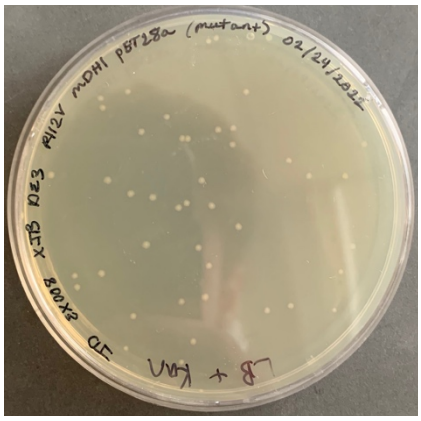

Figure 7. Transformation of XJb (DE3) cells with mutant R111V pET28a plasmid DNA. Transformed XJb (DE3) colonies resulting after overnight incubation with limited growth of satellite colonies.

Table 3

Absorbances of each eluent from Ni-NTA chromatography for R111V MDH1-3 protein purification

Elution step	Absorbance at 280 nm
WASH (1) - 8X resin-bed volumes[a] PBS with 10 mM imidazole	0.38
WASH (2) - 8X resin-bed volumes PBS with 10 mM imidazole	0.28
WASH (3) - 8X resin-bed volumes PBS with 10 mM imidazole	0.067
ELUTION (4) - 2X resin-bed volumes PBS with 250 mM imidazole	2.67

[a]1X resin bed volume = 2 mL

Estimating concentration of collected mutant MDH1-3 protein by BCA assay

The concentration of collected R111V MDH1-3 protein was estimated by BCA assay to prepare for SDS-PAGE (11). Absorbances of the BCA standards at 562 nm show a linear trend when plotted versus BCA standard concentration, with a LINEST analysis providing a standard curve of

$$y = 1.17x + 0.186$$

and an R^2 value of 0.992 (Fig. 8*A*). From the line of best fit, the concentration of the protein sample was averaged to be 1.0 ± 0.1 mg/mL.

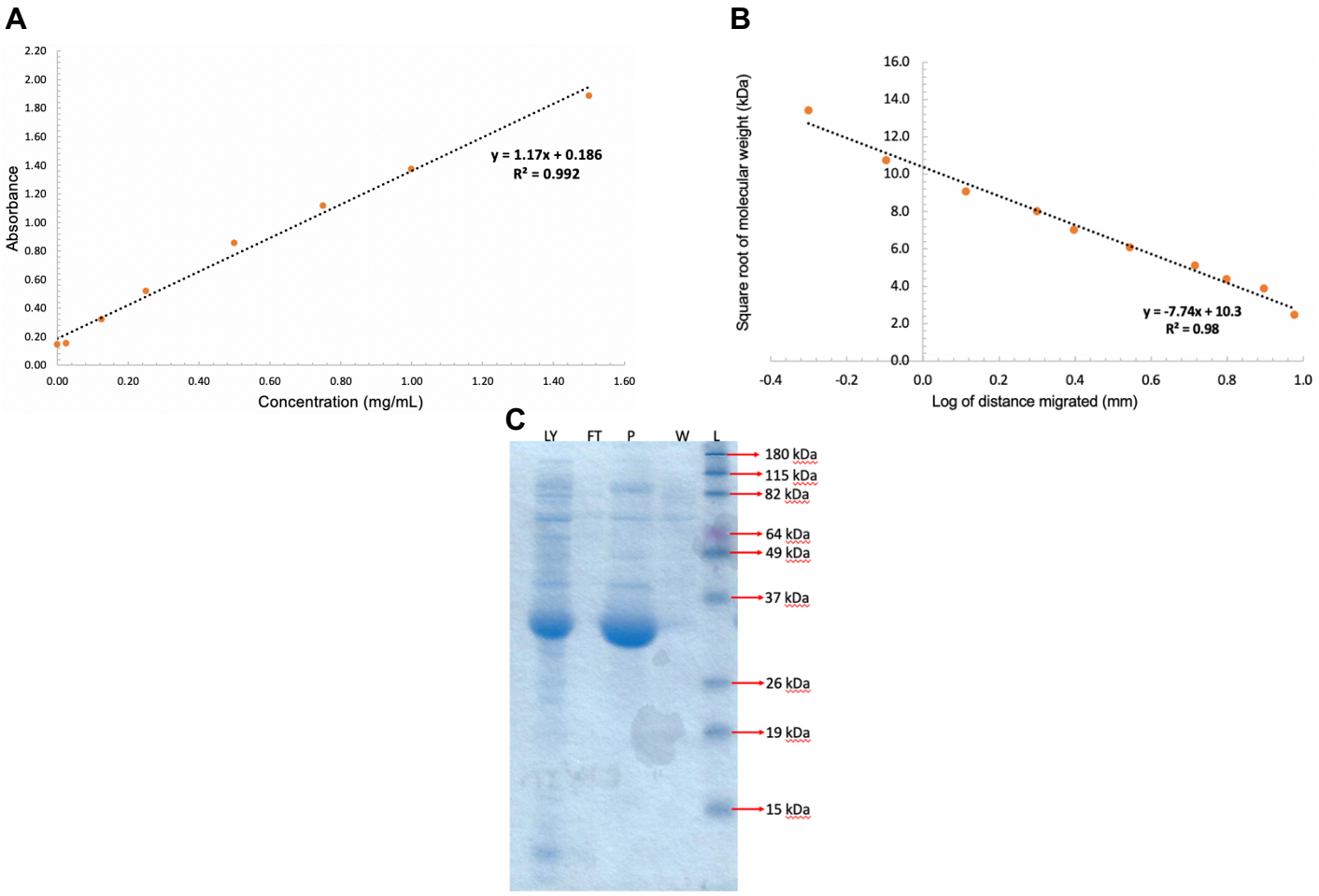

Figure 8. Analysis of collected protein sample by BCA assay and SDS-PAGE. *A,* Absorbances of the prepared BCA standards from measured at 562 nm. The curve was prepared by LINEST analysis and demonstrates an appropriate R^2 value. Migrations of benchmarks were used to prepare a standard curve, *B,* used to estimate the molecular weight of the collected protein sample to confirm its identify as R111V MDH1-3. Standard curve presents an acceptable R^2 by LINEST analysis. *C,* SDS-PAGE of lysate (LY), flow through (FT), protein eluent (P), wash (W), and benchmark ladder *(L).*

Analyzing purified mutant MDH1-3 protein by SDS-PAGE

In order to verify that the protein sample collected by Ni-NTA chromatography is the R111V MDH1-3 protein, the collected sample was analyzed by SDS-PAGE in comparison to the Benchmark pre-stained ladder to confirm the molecular weight (Fig. 8*C*).

To extrapolate the molecular weight of the purified protein, a standard curve was prepared by plotting the square root of the molecular weights for each standard (kD) versus the log of the distance migrated (mm) (Fig. 8*B*). From this, a linear regression analysis provided a line of best fit of

$$y = -7.747 + 10.376$$

with an R^2 value of 0.986. The molecular weight of the collected protein was then extrapolated to be 30.7 kDa, a value within reasonable range to the literature molecular weight of R111V MDH1-3 at 39700 Da.

R111V and wild type MDH1-3 enzyme activity upon preferred substrate oxaloacetate

Kinetic assays for wild type and mutant R111V MDH1-3 were completed using oxaloacetate (OAA) and NADH as substrates to assess the kinetic constants of each enzyme. Using Mathematica, the calculated k_{obs} of the mutant and wild type enzymes were fit against substrate concentration to determine the kinetic constants, k_{cat}, K_M, and k_{sp} (Fig. 9*A,B*). As apparent in both curves, the data collected for mutant enzyme present a much better fit compared to wild type, although the curve is still sufficient to calculate the kinetic constants.

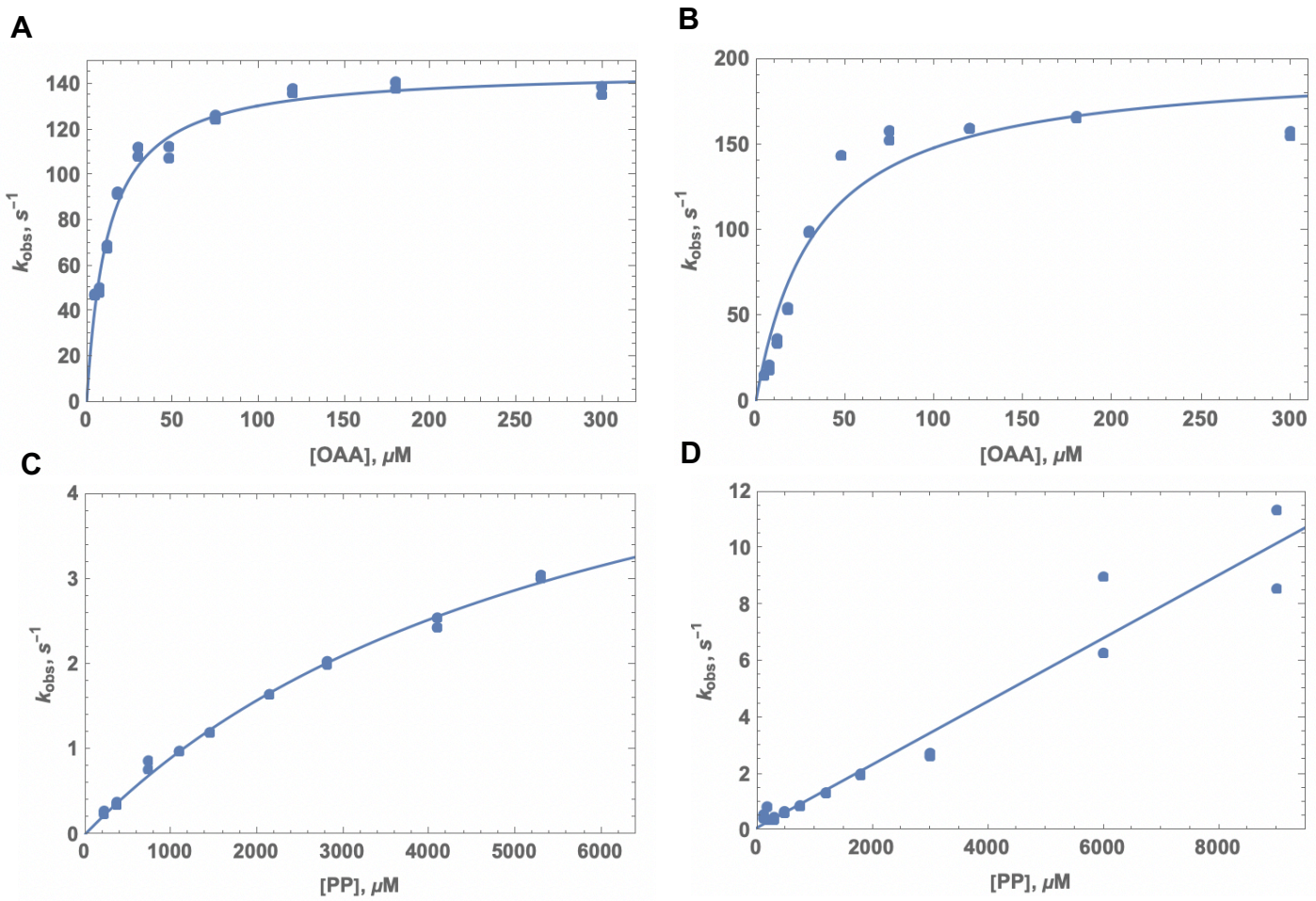

Figure 9. Kinetic curves for mutant R111V and wild type MDH1-3 upon substrates OAA and phenylpyruvate. *A,* Michaelis-Menten kinetic trace for R111V MDH1-3 for varying OAA concentrations compared to *B*, kinetic trace for wild-type MDH1-3 using OAA. *C*, kinetic trace for R111V MDH1-3 presented a better hyperbolic fit compared to that of wild type, *D,* when using phenylpyruvate as substrate (requiring linear fit instead). All curves were prepared on Wolfram Mathematica software.

The data collected during these studies indicate that the wild type enzyme has an enzymatic specificity constant, (k_{sp} = 5.9 ± 0.1 × 10^7 $M^{-1}s^{-1}$) greater than mutant R111V MDH1-3 (k_{sp} = 1.2 ± 0.1 × 10^7) for substrate OAA, as shown in Table 4. The data also suggest that the mutant protein has a slightly lower maximum turnover, k_{cat}, compared to the wild type, demonstrating that it catalyzes less efficiently at lower substrate concentrations. However, both wild type and the mutant MDH1-3 present very high catalytic efficiencies overall at magnitudes of 10^7 $M^{-1}s^{-1}$.

The mutant enzyme also presents a lower K_M value as well, which may indicate that it requires a lower concentration of OAA to reach half maximal velocity. Taken altogether, this data suggest that the R111V mutation has an effect on the kinetic parameters of the enzyme for preferred substrate, OAA.

Table 4

Kinetic constants of mutant R111V and wild type MDH1-3 using OAA as substrate with NADH

Rate constant	Cofactor[a]	Mutant R111V MDH1-3	WT MDH1-3
k_{sp} ($M^{-1}s^{-1}$)	NADH	1.2 ± 0.1 × 10^7	5.9 ± 0.1 × 10^7
k_{cat} (s^{-1})	NADH	150 ± 4	200 ± 20
K_M (μM)	NADH	12 ± 1	30 ± 7

[a]Conditions in 100 mM sodium phosphate buffer at pH 7.4

R111V and wild type MDH1-3 enzymatic activity upon non-preferred substrate phenylpyruvate

In order to further characterize the kinetic profile of R111V MDH1-3, kinetic studies using phenylpyruvate (PP), the non-preferred substrate of MDH1-3, were carried out for both mutant and wild type enzyme.

The kinetic constants were determined after fitting the collected data in the same approach as done for substrate OAA (Fig. 9*C,D*). The data collected for wild-type MDH1-3 did not conform to a hyperbolic fit, instead requiring a

linear fit to determine the specificity constant, k_{sp}, which presents a larger associated error as shown in Table 5.

Table 5

Kinetic constants of mutant R111V and wild type MDH1-3 using PP as substrate with NADH

Rate constant	Cofactor[a]	Mutant R111V MDH1-3	WT MDH1-3
k_{sp} ($M^{-1}s^{-1}$)	NADH	1050 ± 50	$1.1 \pm 0.1 \times 10^3$
k_{cat} (s^{-1})	NADH	6.3 ± 0.4	-
K_M (μM)	NADH	6000 ± 400	-

[a]Conditions in 100 mM sodium phosphate buffer at pH 7.

Expectedly, the mutant MDH1 and wild type enzymes present lower enzyme specificities for the non-preferred substrate, phenylpyruvate, compared to that for OAA. Additionally, mutant R111V MDH1-3 shows a catalytic efficiency for phenylpyruvate close to that presented by the wild type, as shown in comparable k_{sp} values.

Assessing wild type enzyme activity upon OAA by Hill plot

When examining the fitted curve of the wild type enzyme (Fig. 9*B*), it may be proposed that the data conforms to a sigmoidal curve as opposed to the hyperbola model, suggesting that the enzyme acts cooperatively between subunits. In order to justify this observation, the data was fit to a Hill plot to determine the Hill coefficient, n (Fig. 10). As illustrated in the plot, the data fits sufficiently to a sigmoidal curve, presenting a Hill coefficient greater than 1, (n = 2).

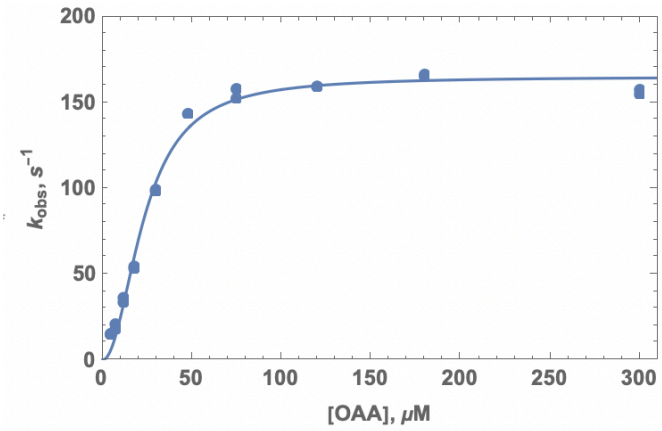

Figure 10. Hill plot of wild type MDH1-3 using OAA as substrate. Wild type MDH1-3 kinetic data using OAA as substrate was fitted to a Hill plot, emphasizing its sigmoidal shape. The plot was fitted using Wolfram Mathematica.

Discussion

As previous literature suggests, cytosolic malate dehydrogenase has been observed to play a role in the upregulated anaerobic fermentation seen in cancerous cells by providing an alternative source of NAD^+ regeneration, thereby increasing glycolytic flux to further support biomass synthesis and cell proliferation. To expand our understanding of how mutagenesis to this enzyme can contribute to changes in the enzyme's behavior, specifically its efficiency and specificity for substrate OAA and non-preferred substrates such as phenylpyruvate, we carried out a mutagenic study by purifying and characterizing mutant R111V MDH1-3. The R111 residue was particularly chosen due to its proximity to conserved residues that play roles in catalysis and substrate binding identified in a multiple sequence alignment with variants of MDH1-3.

Before beginning the purification and enzymatic characterization of mutant R111V MDH1-3, the enzyme was computationally folded with Alpha Fold and simulated on Swiss Dock for phenylpyruvate docking. This molecular modeling did not provide significant differences in the free energy changes, ΔG, associated with phenylpyruvate binding to mutant R111V and wild type MDH1-3. Unexpectedly, predicted ΔG values for OAA binding to wild type were also not significantly different from phenylpyruvate docking to both wild type and mutant enzyme. This computational data conflicted with our expectation that a mutation to the flexible active loop, particularly replacing the large and positively charged Arg 111 with small and hydrophobic valine, would cause a decrease in enzyme substrate discrimination.

In order to assess these computational predictions, we successfully purified from overexpressing XJb (DE3) cells, transformed with mutant plasmid, R111V MDH1-3 enzyme by Ni-NTA chromatography and confirmed purification by BCA assay and SDS-PAGE. We demonstrate by kinetic analysis that this mutation does not increase catalytic efficiency, as shown by an 80% decrease in k_{sp} and 25% decrease in k_{cat} for substrate OAA between wild type and mutant enzymes. However, the decrease in k_{sp} exhibited by the mutant enzyme does suggest a reduced enzyme substrate specificity for OAA, which may have consequences for enzyme activity in the context of glycolytic flux.

To further explore how the mutation affects substrate specificity, we analyzed an alternative catalysis using non-preferred substrate, phenylpyruvate. As expected,

we observed lower k_{sp} values presented by wild type and mutant enzymes compared to those using OAA. This reflects that phenylpyruvate is a non-preferred substrate for MDH1-3. Nonetheless, the mutant and wild type enzymes still present enzymatic activity with phenylpyruvate, which emphasizes the importance of considering alternative substrates as a source for increased NAD^+ regeneration in cancerous conditions.

An unexpected observation of this study is the sigmoidal shape presented in the kinetic trace of wild type enzyme with OAA (Fig. 10*B*). It is reported in literature that cytosolic MDH catalyzes in a non-cooperative manner between its subunits. However, our kinetic trace fits well to a sigmoidal curve with a Hill coefficient, n, greater than 1 (n = 2). This is suggestive of a cooperative mechanism utilized by the wild-type MDH1-3, which challenges preceding studies of the MDH1 catalytic mechanism that have characterized it as non-cooperative. In order to further explore this possibility, more kinetic testing for substrate OAA will need to be carried out for the wild type MDH1-3 enzyme.

The kinetic analysis of mutant R111V presented herein emphasizes that the mutation affects the kinetic parameters for catalysis upon substrate OAA, and less significantly for phenylpyruvate. Initially, it was proposed that substitution of the positively charged Arg 111, which neighbors residue R110 (involved in OAA binding), with the small and hydrophobic valine would create more space within the active site for binding of the larger substrate, phenylpyruvate. Although highly conserved catalytic residues of MDH1-3 were marked as immutable for this study, the R111V mutation induced changes in the acidic environments of these mutations as calculated by H++, possibly providing a rationale for the observed changes in kinetic parameters seen for wild type and mutant enzyme upon OAA.

When considering the H++ data, special attention was directed to residues hypothesized to be involved in the catalytic mechanism, particularly D60, R116, D177, R180, and H205. In wild type MDH1, OAA binds the active site with the help of residues R110 and R180, with R116 stabilizing the transition state. Residues D177 and H205 form the catalytic dyad for H205 to act as both an acid and base catalyst. Meanwhile, co-substrate NAD^+ binds with the help of D60 through hydrogen bonds to the 2' and 3' hydroxyl groups, forming a ternary structure between H205, R110, R180, and D60, that prompts a conformational change to the active flexible loop to shield the substrates from solvent (12). As estimated in the H++ computational data, these residues experience changes in their pK_a values due to the R111V mutation. Most notable are the increases in pK_a values calculated for D177 and D60, indicating lower acidic strengths. Oppositely, residues H205 and R180 experience a decrease in pK_a, suggestive of a higher acidic strength. The changes in proton binding affinities may rationalize the lower enzyme specificity and catalytic efficiency observed for mutant R111V MDH1-3 compared to the wild type for substrate OAA given the potential disruption to catalytically active residues. Interestingly, these changes did not appear to affect the kinetic parameters as significantly for non-preferred substrate phenylpyruvate between wild type and mutant enzyme.

While these results provide preliminary data for the characterization of mutant R111V MDH1-3 enzyme, kinetic studies of the wild type enzyme using phenylpyruvate and OAA must be repeated to provide reliable comparisons to the mutant R111V, given its poor fit to the hyperbolic model, and to further support the determination of the Hill coefficient. Additionally, in order to comprehensively assess changes in enzyme substrate specificity for the mutant enzyme, a range of naturally occurring, alternative substrates with structures mimicking that of natural substrate OAA should be considered for kinetic testing. This could provide more revealing information in how exactly MDH1 activity is upregulated in cancerous states.

In conclusion, the findings in this report emphasize the importance of examining cytosolic MDH as a contributor to NAD^+ regeneration and thus, increased cell proliferation. Importantly, we show that mutation to residue R111 can induce changes to MDH1 kinetic behavior that affect enzyme efficiency and substrate specificity. Although the R111V mutation does not produce an increase in catalytic efficiency for either substrate, there are still observed changes to enzyme specificity that highlight the important link between mutations of this type and altered enzyme activity, which may have important implications in the progression of cancer.

Experimental procedures

Multiple sequence alignment of human cMDH1 gene and PyMOL modeling

To select and model the mutation for MDH1-3, a multiple sequence alignment was performed using several variants of the cytosolic MDH enzyme. The human cMDH1 gene was specifically aligned with multiple

reviewed cMDH1 genes from a diverse set of genera. Conserved residues throughout the cMDH1 gene were subsequently identified from the alignment and marked as immutable for site directed mutagenesis.

cMDH1 was then modeled on PyMOL for visualization of both the active site and flexible loop using malate and NAD^+ as substrates. Residue Arg 111 was chosen for mutation due to its orientation within the flexible loop region and proximity to R110, which plays a significant role in OAA binding. Selection of the residue was followed by simulated site directed mutagenesis to valine using the mutagenesis tool offered by PyMOL. This mutation was chosen based on the rationale that a smaller amino acid in place of the Arg 111 would expand space in the active site for the larger phenylpyruvate to bind.

Using Alpha Fold for and SwissDock for phenylpyruvate docking to R111V MDH1-3

The Alpha Fold software was utilized to model the R111V MDH1-3 mutant protein and develop a predicted structure. In order to identify the regions of interest for phenylpyruvate simulated docking, average distances between His 205 and Ser 159 were measured for X, Y, and Z coordinates of the heterocycle nitrogen and side chain oxygen in PyMOL. These residues were chosen due to their proximity to the active site.

With these coordinates, the PDB file was uploaded to SwissDock for simulated docking of phenylpyruvate. The accurate docking type and option 3 for flexibility were chosen for this simulation. The resulting file was then opened with Chimera in order to choose clusters of interest that might accurately depict phenylpyruvate modeling.

After identification of appropriate clusters, ΔG energies were averaged using the provided CSV file and compared to those resulting from wild type phenylpyruvate and oxaloacetate docking.

Analyzing changes in pK_a *of titratable residues with H++*

In order to examine changes in the pK_a values of titratable residues due to the R11V mutation, the mutant and wild type protein structures (folded by Alpha Fold) were processed by H++. The pK_a values of residues involved in catalysis, substrate binding, and those neighboring the R111 position were considered for computing ΔpK_a values (wild type – mutant).

Preparation of E. coli BL21 (DE3) strain liquid cultures

E. coli BL21 (DE3) cells harboring pET28a plasmid encoding the cMDH1 gene (isoform 3; UniProt code P40925-3) were a generous gift from Dr. Jessica Bell from the Department of Chemistry and Biochemistry at the University of San Diego. Plates containing Luria Bertani (LB) with kanamycin (3% agar, 1% tryptone, 0.5% yeast extract, 1% sodium chloride, and 50 µg/mL kanamycin at pH 7) were streaked from frozen glycerol stocks of the BL21 (DE3) strain and grown at 37°C overnight. Using a colony populated plate, 10 mL of LB medium with kanamycin were inoculated with a single colony and grown overnight at 28°C with shaking at 250 rpm. To ensure proper growth, the optical density at 600 nm was confirmed to be between 2.0-3.5. The resulting cultures were then pelleted by centrifugation at 16,000 × g and frozen at -20°C.

Plasmid miniprep using Zymo Research Zyppy miniprep kit

To isolate pET28a MDH1-3 plasmid from cultured *E. coli* BL21 (DE3) cells, 3 mL of liquid culture were processed according to the manufacturer's protocol as outlined in the Zyppy™ miniprep kit (Zymo, Plasmid Miniprep Kit, Cat.#: D4019). An additional wash with absolute ethanol was incorporated into the protocol following the Zyppy wash buffer. The plasmid DNA was then eluted using heated Zyppy elution buffer (to 50°C), consisting of 10 mM Tris and 0.1 M EDTA at pH 8.5 and the concentration determined via Nanodrop™.

Plasmid DNA restriction digest

For the purposes of analyzing the collected plasmid DNA, a double restriction digest was performed with 1 µg of DNA, 3.1 NEB buffer, and 10 units each of BglI (New England Biolabs, Cat.#: R0143S) and NcoI (NEB, Cat.#: R3193S) restriction enzymes to a total volume of 25 µL. The reactions were incubated at 37°C and treated with loading dye for gel electrophoresis.

Reaction samples were loaded onto a 1% agarose gel prepared with TBE (89 mM Tris base, 89 mM boric acid, and 2 mM EDTA at pH 7.6), which was then run at 80V for 1 hour.

Designing primers for site directed mutagenesis using NEB Base Builder

After selection of the R111V mutation, primers compatible with NEB's Q5 site-directed mutagenesis kit were designed using the NEBaseChanger™ tool.

Before initiating primer design, a specific mutation to the nucleotide codon for R111 on the coding strand of the MDH1-3 gene was selected based on *E. coli* codon frequencies. Given that the most frequent codon expressed for valine by *E. coli* is GTG, and the wild type R111 codon is AGG, the first two nucleotides were mutated to GT.

With this mutation, the complete FASTA sequence corresponding to MDH1-3 pET28a was uploaded to the NEBaseChanger™ tool, along with the desired nucleotide substitutions, producing a forward primer of 25 nucleotides in length, and an 18-nucleotide long reverse primer with sequences displayed below:

```
F_5'…CATGCCAAGAgtGGAAGGCATGGAG…3'
R_3'….       GAGCCCACAAGAATGGCC…5'
```

Site directed mutagenesis of MDH1 pET28a using designed primers followed by KLD treatment

Site directed mutagenesis for the desired mutation at residue 111 was carried out using the Q5® site directed mutagenesis kit purchased from New England Biolabs (NEB, Cat.#: E0554S), along with the mutant primers. The procedure was followed as outlined in the manufacture's protocol. The reaction mix prepared for this site directed mutagenesis contained the forward and reverse primers at 0.5 µM concentrations, as well as pET28a plasmid DNA at a concentration of 25 ng/µL.

To carry out PCR using the mutagenic primers, initial denaturation at 98°C took place for 30 seconds. The program was then set for 30 cycles, each consisting of denaturation at 98°C for 10 seconds, primer annealing (carried out at a temperature closest to 62°C – suggested by NEB) at 62.3°C for 30 seconds, and extension at 72°C for 2.5 minutes. Following 30 cycles, the final extension was carried out at 72°C for 2 minutes.

PCR results were then analyzed on a 1% agarose gel prepared with TBE (89 mM Tris base, 89 mM boric acid, and 2 mM EDTA at pH 7.6), which was run at 80 V for 1 hour and compared to a 1kb+ ladder.

The PCR product of mutant R111V MDH1 pET28a plasmid DNA prepared from the mutagenesis procedure was subject to a kinase, ligase, and DpnI treatment, which was carried out according to the manufacturer's protocol.

The resulting KLD mixture was then used to transform competent NEB 5-α cells. To a sample of thawed cells, 5 µL of KLD mixture were added and the cells incubated on ice for 30 minutes. Following this incubation, cells were then subject to heat shock at 42°C for 30 seconds and then again incubated on ice for 5 minutes. To the transformation mixture, 900 µL of room temperature SOC were added and the contents incubated at 37°C with shaking at 175 rpm.

The transformation mixture was then grown on plates containing LB with kanamycin (3% agar, 1% tryptone, 0.5% yeast extract, 1% sodium chloride, and 50 µg/mL kanamycin at pH 7) in 100 µL aliquots (one plate was spread with 100 µL of diluted transformation mixture).

Preparation of transformed NEB 5-α competent E. coli liquid cultures

Using colonies of NEB 5-α cells transformed with mutant MDH1 pET28a plasmid from the KLD treatment procedure, 5 mL of LB medium with kanamycin added (1% tryptone, 0.5% yeast extract, and 1% sodium chloride, and 50 µg/mL kanamycin at pH 7) were inoculated with a single colony. Cultures were grown at 28°C with shaking at 250 rpm. Before moving onto the plasmid miniprep procedure, the optical density at 600 nm was ensured to be within 0.2-0.35 via 1/10 dilution of liquid culture with LB and kanamycin media.

Plasmid miniprep of mutant MDH1 pET28a plasmid using Zymo Research Zyppy miniprep kit

Isolating the mutant R111V MDH1 pET28a plasmid took place via plasmid minipreparation once again using the Zymo Research Zyppy Plasmid Miniprep kit as explained above for the wild type. The procedure was followed as outlined in the manufacturer's protocol, except for an additional wash step and the elution process. Following wash with Zyppy Wash Buffer, the column was washed with absolute ethanol and centrifuged at 16,000 × g for 30 seconds.

To ensure that the plasmid DNA sample was suitable for sequencing, the DNA was eluted from spin columns using 10 mM Tris buffer at pH 7.5. Before addition to the column, the buffer was warmed to 50°C and once added, was incubated on the column for 10 minutes before centrifugation at 16,000 × g for 30 seconds. The eluted

plasmid DNA was analyzed by Nanodrop™ to ensure an appropriate concentration for sequencing.

Preparation of mutant MDH1 plasmid for sequencing by GeneWiz

To prepare samples of mutant R111V MDH1-3 DNA for sequencing by GeneWiz, the sample guidelines as laid out by the manufacturer were followed.

The T7 universal primer offered by GeneWiz was selected for sequencing due to its annealing locations in proximity to the R111V MDH1-3 mutation on the pET28a plasmid.

Transformation of competent XJb (DE3) E. coli cells using mutant MDH1 plasmid

Once it was confirmed that the mutagenesis procedure was successful in introducing the R111V mutation to the pET28a MDH1-3 plasmid, a transformation protocol with XJb (DE3) cells was carried out to prepare for overexpression. Before beginning the protocol, plates containing LB and kanamycin were warmed at 37°C.

The Z-competent XJb (DE3) cells were first obtained from Zymo and carefully thawed on ice (Zymo, Mix and Go! XJb Autolysis Competent Cells, Cat.#: T3051). From each tube, 50 µL of cells were removed to maximize transformation efficiency. To each sample, 100 ng of mutant R111V MDH1-3 pET28a plasmid DNA were added and the contents mixed gently. The cells were then incubated for 10 minutes on ice. Subsequently, 4 volumes of SOC outgrowth media were added, followed by incubation at 37°C with gentle shaking. Transformation mixtures were then plated on the prewarmed LB and kanamycin plates, which were incubated at 37°C for no longer than 18 hours to prevent growth of satellite colonies.

Preparation of transformed XJb (DE3) E. coli liquid cultures

For use in the cell lysis procedure, liquid cultures of XJb (DE3) cells transformed with mutant R111V MDH1-3 pET28a plasmid were prepared by inoculating 6 mL of LB and kanamycin media with single colonies. Cultures were grown overnight at 37°C with shaking at 250 rpm. The OD_{600} of the resulting cultures were confirmed to be within the 4.0-5.0 range prior to beginning the overexpression procedure.

Protein overexpression of mutant R111V MDH1-3 in XJb (DE3)

To overexpress the mutant R111V MDH1-3 protein, liquid cultures of XJb (DE3) cells expressing the R111V MDH1-3 pET28a plasmid were expanded to 50 mL with LB and kanamycin media. The volume of liquid culture added to the media was ensured to provide a starting OD_{600} between 0.04 and 0.05. The expansion was then incubated at 37°C with shaking at 250 rpm until the culture reached a final OD_{600} between 0.55-0.6.

Once the appropriate reading was reached, the culture was cooled down to room temperature for the addition of IPTG and arabinose to final concentrations of 0.5 mM and 3 mM, respectively. The cultures were then grown for 12-18 hours at 20°C with vigorous shaking at 250 rpm and then harvested by centrifugation at 3,000 × g at 4°C for 10 minutes.

Cell lysis of XJb (DE3) cells overexpressing mutant MDH1-3 protein

Immediately following harvest of pelleted XJb (DE3) cells overexpressing mutant R111V MDH1-3 protein, cells were resuspended in 3 mL of lysis buffer consisting of 20 mM Tris, and 100 mM NaCl at pH 8 (the amount added conferred to the ratio of 3 mL lysis buffer/g cell pellet) to begin the protein purification process. Before addition of the lysis buffer, Pierce™ protease cocktail inhibitor tablets were added to the buffer in an amount of 1 tablet per 10 mL buffer (Thermo Scientific™, Pierce™ Protease Inhibitor Tablets, Cat.#: A32955). The pellet was then frozen at -20°C until starting two freeze-thaw cycles with liquid nitrogen to improve the efficiency of cell lysis.

After completely resuspending pellets, lysozyme and DNAse I were added to concentrations of 1 mg/mL and 0.02 U/µL, respectively. Incubation of the mixture then followed at 37° with shaking at 200 rpm until homogenous.

The resulting sample was then subject to centrifugation at 15,000 × g for 30 minutes at 4°C and a portion of the supernatant (from here, on referred to as lysate) was stored at -20°C for downstream analysis.

Purification of mutant MDH1-3 protein by Ni-NTA affinity chromatography

Ni-NTA resin was first equilibrated with equilibration buffer (PBS, 20 mM sodium phosphate, and 300 mM sodium chloride at pH 7.4) according to the manufacturer's protocol (Thermo Scientific™, HisPur Ni-

NTA resin, Cat.#: 88221). The resin and equilibration buffer were centrifuged at a speed less than 800 × g for 1 minute and the supernatant removed (13).

The cell lysate sample resulting from the lysis procedure was then added to the resin, which possessed a binding capacity of less than 60 mg of His-tagged protein/mL. The resin was mixed on an end-over-end rotator for 30 minutes at 4°C and poured in the column for chromatography.

Once added, the resin was washed with buffer containing PBS with 10 mM imidazole until a specific A_{280} was reached. The bound protein was eluted using a one resin-bed volume of PBS with 250 mM imidazole.

Determining concentration of mutant MDH1-3 protein sample by bicinchoninic acid assay

Preparation of BCA standards from BCA stock solution, as well as the working reagent, took place according to the manufacturer's protocol (Thermo Scientific™, Pierce™ BCA Protein Assay Kit, Cat.#: 23225) .

The standards and mutant R111V MDH1-3 were then aliquoted in 50 µL amounts to 1 mL samples of working reagent and then incubated at 37°C with gentle shaking for 30 minutes. Absorbances were recorded at 562 nm to determine the concentration of mutant protein in the sample collected by Ni-NTA chromatography.

Analyzing mutant MDH1-3 protein sample by SDS PAGE

The collected R111V MDH1-3 mutant protein sample was analyzed by SDS-PAGE using the method of Laemmli with exception of sample buffer, which contained 2 mM DTT for each sample and 1% β-mercaptoethanol as opposed to 5% (14).

Stacking and separating gels were ran at 55 mA and 30 mA, respectively. The gel was then stained with Coomassie Blue (0.1% Coomassie Blue R-250 in 40% ethanol, and 10% acetic acid) for approximately 3 hours and placed on an orbital shaker at 80 rpm. Destaining was carried out with 40% methanol, 10% acetic acid, and 30% glycerol.

The gels were dried at 80°C for approximately 2 hours under vacuum before temperature was turned down to room temperature to dry for an additional hour.

Testing for R111V MDH1-3 kinetic activity with substrates oxaloacetate, phenylpyruvate, and NADH

Kinetic assays were completed in assay buffer consisting of 0.152 mM NADH in 100 mM potassium phosphate buffer at pH 7.4. OAA stock solutions of 45 mM and 4.5 mM in water were used as enzyme substrate. In each assay, final concentrations of NADH and enzyme were 150 µM and 8 nM, respectively. Final concentrations of OAA ranged from 3.8-300 µM to field a sufficient spectrum of enzyme activity.

Kinetic assays using phenylpyruvate were prepared in the same assay buffer with final NADH concentrations of 150 µM. Final concentrations of enzyme and phenylpyruvate within the assay ranged from 78-69 nM and 224-5976 µM, respectively.

Enzyme activity was initiated by adding substrate to the assay and the change in absorbance was measured at 340 nm for 30 seconds at room temperature to monitor the consumption of NADH. Absorbances were measured with the Agilent Cary 3500 UV-Vis spectrophotometer. The enzyme turnover number at each substrate concentration were fitted using Wolfram Mathematica and the kinetic constants calculated using the modified method proposed by Johnson (15).

Acknowledgements – This work was completed with the guidance and direction of the MDH CURE Community (MCC) and we thank the program for inviting Providence College to be a member. We thank the Department of Chemistry and Biochemistry and the chair, Dr. Kenneth Overly. We extend our gratitude to the Department of Biology, especially Dr. Brett Pellock, for lending the use of lab equipment and instruments. We appreciate New England Biolabs for their donation of restriction enzymes. We are also grateful to the faculty at the University of San Diego, particularly Dr. Jessica Bell and Dr. Joseph Provost for providing E. coli BL21 (DE3) cells harboring pET28a plasmids expressing hMDH1 and constructing MDH models, respectively. Finally, we thank the members of the CHM 310 laboratory course as an entity for their remarkable work in completing this project.

References

1. Heiden, M. G. V., Cantley, L. C., Thomson, and C. B. (2009) Understanding the Warburg Effect: the metabolic requirements of cell proliferation. *Science* **324**, 1029-1033

2. Hanse, E., Kachman, M., Wang, D., Lowman, X., and Kelekar, A. (2017) Cytosolic malate dehydrogenase activity helps support glycolysis in actively proliferating cells and cancer. *Oncogene* **36**, 3915-3924
3. Zhang, B., Tornmalm, J., Widengren, J., Vakifahmetoglu-Norberg, H., and Norberg E. (2017) Characterization of the role of the malate dehydrogenases to lung tumor cell survival. *J. cancer*. **8**, 2088-2096
4. Mansouri, S., Shahriari, A., Kalantar, H., Zanjani, T., and Karamallah, M. (2017) Role of malate dehydrogenase in facilitating lactate dehydrogenase to support the glycolysis pathways in tumors. *Biomed. Rep*. **6**, 463-467
5. The UniProt Consortium (2020) UniProt: the universal protein knowledgebase in 2021. *Nucleic Acids Res.* **49**, D480-D489
6. The PyMOL Molecular Graphics System, Version 2.0 Schrödinger, LLC
7. Jumper, J., Evans, R., Pritzel, A., Green, T., Figurnov, M., Ronneberger, O., Tunyasuvunakool, K., Bates, R., Žídek, A., Potapenko, A., Bridgland, A., Meyer, C., Kohl, S., Ballard, A., Cowie, A., Romera-Paredes, B., Nikolov, S., Jain, R., Alder, J., Back, T., Petersen, S., Reiman, D., Clancy, E., Zielinski, M., Steinegger, M., Pacholska, M., Berghammer, T., Bodenstein, S., Silver, D., Vinyals, O., Senior, A., Kavukcuoglu, K., Kohli, P., Hassibis, D. (2021) Highly accurate protein structure prediction with Alpha Fold. *Nature* **596**, 583-589
8. Grosdidier, A., Zoete, V., Michielin, O. (2011) SwissDock, a protein-small molecule docking web service based on EADock DSS. *Nucleic Acids Res.* **39,** W270-W277
9. Pettersen, E. F., Goddard, T. D., Huang, C. C., Couch, G. S., Greenblatt, D. M., Meng, E. C., Ferrin, T. E. (2004) UCSF Chimera – a visualization system for exploratory research and analysis. *J. Comput. Chem*. **25**, 1605-1612
10. Anandakrishnan, R., Aguilar, B., Onufriev, A. V. (2012) H++ 3.0: automating p*K* prediction and the preparation of biomolecular structures for atomistic molecular modeling and simulations. *Nucleic Acids Res*. **40**, W537-W541
11. Smith, P. K., Krohn, R. I., Hermanson, G. T., Mallia, A. K., Gartner, F. H., Provenzano, M. D., Fujimoto, E. K., Goeke, N. M., Olson, B. J., Klenk, D. C. (1985) Measurement of protein using bicinchoninic acid. *Anal. Biochem*. **150**, 76-85
12. Minárik, P., Tomášková, N., Kollárová, M., and Antalík, M. (2002) Malate dehydrogenases – structure and function. *Gen. Physiol. Biophys*. **21**, 257-265
13. Block, H., Maertens, B., Spriestersbach, A., Brinker, N., Kubicek, J., Fabis, R., Labahn, J., Schäfer, F. (2009) Immobilized-metal affinity chromatography (IMAC): a review. *Meth. Enzymol.* **463**, 439-473
14. Laemmli, U. K. (1970) Cleavage of structural proteins during the assembly of the head of bacteriophage T4. *Nature* **227,** 680-685
15. Johnson, K. A. (2019) New standards for collecting and fitting steady state kinetic data. *J. Org. Chem*. **15**, 16-29